AAS 10-268

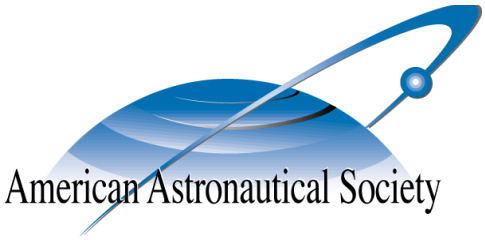



American Institute of
Aeronautics and Astronautics

# IMPACT OF NODAL ATTITUDE MOTION ON TWO-ELEMENT TETHERED COULOMB STRUCTURES

**Carl R. Seubert and Hanspeter Schaub**

**AAS/AIAA Space Flight Mechanics Conference**

**San Diego, CA** **February 14–18, 2010**

**AAS Publications Office, P.O. Box 28130, San Diego, CA 92198**

(Preprint) AAS 10-268

# IMPACT OF NODAL ATTITUDE MOTION ON TWO-ELEMENT TETHERED COULOMB STRUCTURES

**Carl R. Seubert*** **and Hanspeter Schaub†**

Combining features of large space structures and free-flying formations has lead to the tethered Coulomb structure (TCS) concept. Utilizing Coulomb forces to repel a formation of spacecraft nodes that are connected with fine tethers can create large quasi-rigid and lightweight space structures. There are numerous applications for a TCS ranging from interferometry and remote sensing to component deployment and inflatable structures. This paper presents the first results on how the nodal attitude motion impacts the TCS concept and required charge levels. Numerical simulations analyze the complex and coupled relative motion, including simple tether dynamic models and TCS node attitude motions. Quantitative analysis shows that increasing the inflationary Coulomb forces can stiffen the entire structure to resist deformations due to initial nodal rotations. This can be achieved while maintaining realistic charge levels. A two node system demonstrates the ability to maintain shape and a taught tether under the disturbance of initial angular rate errors and solar radiation pressure. Further, a simple double-tether system is shown to offer increased stiffening properties and resistance to perturbations.

## INTRODUCTION

The use of spacecraft for remote sensing, interferometry, and telescopic operations is a progressive area of research with large baselines sought to increase power, sensor accuracy and resolution. Large space structures and free-flying spacecraft formations are two active development approaches to address this need.

Large space structures offer a rigid and fixed configuration that may be required for highly accurate observations. Inflatable and deployable systems can offer a low-mass, high mechanical packaging efficiency and potentialy low cost solution that can been used for applications such as antennas and booms.[1,2,3] An ongoing area of research is the development and test of deployable components and material membranes for large space structures.[4] However, there are challenges to overcome prior to large space structures becoming standard operating systems, including large mass, volume and cost constraints to get to orbit, the need for on-orbit construction or complexities and reliability of deployable components.

An alternate method of providing the same characteristics of a large space structure is to use a cluster of spacecraft flying in a desired formation. The proposed NASA Goddard Stellar Imager[5] and the NASA JPL study on the proposed Terrestrial Planet Finder (TPF)[6] are two missions that intend to operate a formation of spacecraft creating a sensor baseline in the kilometer range. One of the leading applications of a large space interferometer is observations from Geostationary Earth Orbit (GEO). A study by Wertz of a GEO-based free-flying formation indicates that an Earth

*Graduate Research Assistant, Aerospace Engineering Sciences Department, University of Colorado, Boulder, CO. AIAA student member, AAS student member

†Associate Professor, H. Joseph Smead Fellow, Aerospace Engineering Sciences Department, University of Colorado, Boulder, CO. AIAA Associate Fellow, AAS member

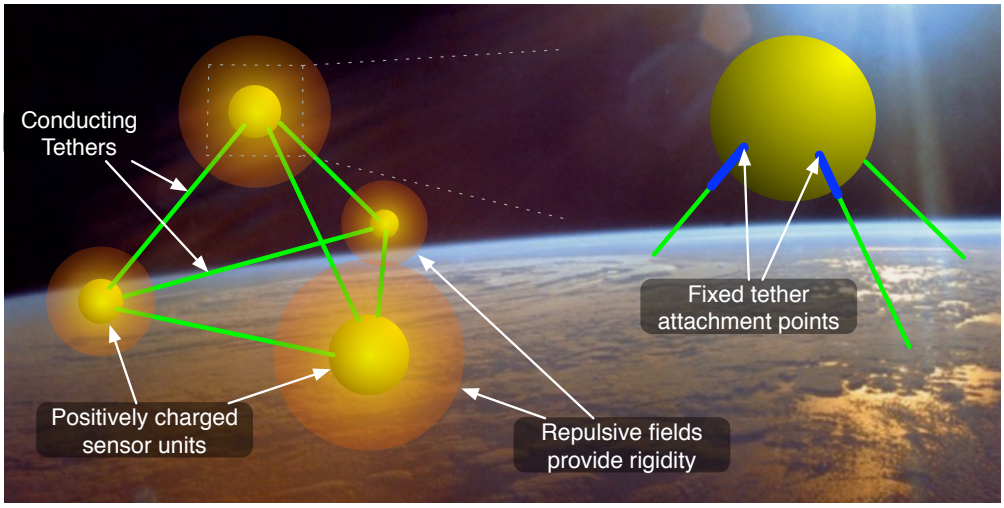


**Figure 1. Illustration of the tethered Coulomb structure concept**

surface resolution of 0.5-2 m is achievable.[7] The Eyeglass concept is another investigation into a GEO-based Earth surveillance platform with a 25-100 m aperture telescope. The diffractive lens is designed to be folded in a sequence similar to a origami layout and will be deployed in orbit.[8,9] King and Parker in Reference 10 investigate the use of Coulomb forces to control a free-flying formation of spacecraft to develop a 20-30 m size array for interferometry at GEO.

One of the biggest challenges of a free flying formation in Earth orbit is controlling the non-linear and strongly coupled relative orbits and achieving the desired cluster geometry. With the use of conventional chemical thrusters there is a limitation of propellant and consequently mission lifetime to maintain a desired formation. With close formations and sensitive instrument missions there are also plume impingement concerns. Two formation control concepts mitigating high fuel expenditure and plume impingement are electromagnetic[11] and flux pinning, both of which require high operational power levels.[12] Coulomb thrust is a recent and novel method to control the separation distance of spacecraft operating in close formations that does not have plume impingement concerns, is virtually propellant-less, and requires only Watt-levels of power.[10,13,14]

One potential solution to achieving a low-mass large space structure is with the Tethered Coulomb Structure (TCS) concept proposed in Reference 13. The TCS provides a hybrid combination of features from space structures and free flying spacecraft formations. The TCS concept utilizes a formation of spacecraft nodes that are held together with a 3D network of light-weight physical tethers. This is in contrast to other Coulomb spacecraft research which investigates the use of virtual tethers using electrostatic forces.[15,16] With the TCS concept each spacecraft node has the ability to increase its electrostatic potential through the use of a charge control device that emits either electrons or low mass ions. With each node having the same charge polarity they will repel from each other and induce a tensile force on each tether. This Coulomb repulsive force essentially inflates the spacecraft structure while the shape and size is maintained by the tethers. An illustration of a four node TCS is shown in Figure 1.

The TCS concept offers a number of advantages for the development of large space structures. Costs are kept low by launching the formation in a compact configuration that is inflated in orbit using the Coulomb forces. Similarly, a deployable component or antenna could essentially be in-

flated and held quasi-rigid from the spacecraft body using Coulomb force repulsion. Due to the micro- to milli-Newton level of Coulomb forces it is only necessary to have a network of small membrane-like tethers. This significantly reduces the TCS mass compared to traditional structural components and does not require on-orbit construction. It is also envisioned that structures as large as hundreds of meters are feasible by connecting multiple charged nodes with relative short and thin tethers (tens of meters). Another key benefit of the concept is its ability to vary the shape and size of the TCS configuration by varying the tether lengths. This allows adaptability and variation for changing mission requirements.

There exists a variety of applications for space tether systems and studies typically utilize a spinning system,[17,18] a gravity gradient or an atmospheric drag orientation to maintain tension.[19,20] A unique advantage of the TCS concept is that tension is provided with Coulomb forces regardless of the orbital orientation and can be used to overcome differential gravitational accelerations and external perturbations.

Controlling a free-flying spacecraft formation with Coulomb forces or traditional methods is an interesting dynamical challenge. On going research in this field includes equilibrium conditions of Coulomb craft,[21,22] implementation of feedback stabilized virtual Coulomb structures with two craft,[23,15,16] and the control of three craft.[24,25] The navigational and dynamical motion complexities of operating tightly controlled free-flying formations are significantly simplified with the TCS concept.

The TCS concept, with its many advantages, still requires further research to address the challenges such as low-tension tether dynamics and deployment mechanisms, the dynamics of charged quasi-rigid structures with independently rotating nodes and variable TCS shape goals, the electrical power requirements to maintain non-equilibrium charge levels, as well as the ability to maintain a delicate TCS structure during orbital maneuvers such are semi-major axis corrections. The intent of this paper is to study how the individual attitude motions of the TCS nodes impact the overall charge requirements. The concern is that a node rotation due to small deployment errors or external torques could cause the tethers to wind up or loose tension. The analysis investigates how the nodal charge impacts the rotational stiffness for a simple two-node TCS configuration. This is an advancement over the previous TCS modeling that used point mass nodes (ignoring nodal attitude motions) and focused on how the overall structure motion and shape changes can be used to stabilize the TCS orientation.[13]

A simple two-node, two degree of freedom (DOF) TCS model is developed. Through linearization, analytic equations of motion are used to offer insight into expected translational and rotational motions including the effects of varying model parameters. Non-linear simulations featuring dynamic tethers modeled as simple, mass-less, proportional and undamped springs are performed. The results of dynamic studies investigating the systems ability to resist deformation from initial angular rate errors or external disturbance forces are presented.

The primary intent of this study is to analyze the ability of the Coulomb force to stiffen the overall TCS structure and resist deformation. This is further demonstrated with the results of reducing the tether length under the presence of attitude rate errors as well as a simple solar radiation pressure perturbation. Another focus of this study is determining the conditions that cause slack tethers, a situation that may lead to damage or entanglement. Further, to enhance the orientational stiffening capabilities of the Coulomb inflationary force, a TCS configuration with a redundant two-tether connection is investigated. Results are generated by numerically simulating the full non-linear

equations of motion for any general three-dimensional TCS size or shape using any number of spacecraft nodes. This algorithm development is shown in the appendix. The presented research results are a vital step for the future analysis of more complex systems and higher fidelity modeling of the TCS relative motion.

## TETHERED COULOMB STRUCTURE FORCES

This section develops the fundamental forces acting on a TCS system. The dynamic model considered includes translational and rotational degrees of freedom of each TCS node, Coulomb forces for inflation, and fixed deployed tether lengths to maintain a constant average size and shape. The TCS shape will undergo small variations due to flexing of the tethers and motion of the nodes.

### Coulomb Force

For the TCS system the Coulomb force is the controllable actuator. This force is generated from the interaction of two charged bodies. The charge can either occur naturally due to interaction with the space plasma, or be driven by a charge control device which continually emits charged particles. In space, this force is reduced by shielding from the free-flying charged particles of the local plasma. The strength of this shielding is defined by the Debye length $\lambda_d$.[26] The Coulomb force $\boldsymbol{F}_c$ that is generated between two craft of charges $q_1$ and $q_2$ is defined by:

$$|\boldsymbol{F}_c| = k_{\mathrm{c}} \frac{q_1 q_2}{x^2} e^{-x/\lambda_d} \left(1 + \frac{x}{\lambda_d}\right) \tag{1}$$

where $x$ is the spacecraft separation distance and $k_c = 8.99 \times 10^9\ \mathrm{C}^{-2}\mathrm{Nm}^2$ is the vacuum Coulomb constant. The Debye length is based on the temperature and density of the local plasma. At GEO the plasma is sufficiently hot and sparse to generate Debye lengths ranging from 80 -1000 m with an average of approximately 200 m, allowing the use of Coulomb thrust when operating with spacecraft separations of dozens of meters at GEO.[14,27] Low Earth orbit Debye lengths are typically cm level, making the use of Coulomb thrust challenging.

For the TCS system the Coulomb force is chosen to be repulsive to provide an inflationary force to maintain tension on the tethers. This is achieved through a positive charge product, $Q = q_1 q_2$, with either both positive or negative $q_i$ values. This study uses spherical spacecraft bodies where a charge level $q$ results in a surface potential computed with the relationship:

$$q = \frac{Vr}{k_c} \tag{2}$$

where $V$ is the voltage and $r$ is sphere radius. Note that this study does not consider non-homogeneous charge distributions that can occur from induced charge effects of two neighboring conducting objects. Such effects will be very small compared to the absolute charge imparted on each node if the node separation distance is multiple times greater than the node radius $r$.

### Tether Force

The tethers are modeled as linear stretch springs that, when in a compressed state, go slack and no force is produced. Consequently they only produce a force that opposes the repulsion of the Coulomb force. The magnitude of the force is governed by the equation:

$$|\boldsymbol{F}_{\mathrm{s}}| = \begin{cases} k_{\mathrm{s}} \delta L & \delta L > 0, \\ 0 & \delta L \leq 0. \end{cases} \tag{3}$$

where $k_s$ is the linear spring constant and $\delta L$ is the stretch in the tether length between two nodes.

One option for a spacecraft tether material is AmberStrand®*. The property values of this reference material is used for all simulations in this paper. AmberStrand® is an electrically conductive hybrid yarn made up of a metal coated polymer that offers a flexible, low-mass and high strength tether. Tests conducted at the University of Colorado at Boulder on a braid of three twisted Amberstrand® fibers resulted in the tether properties shown in Table 1.

**Table 1. AmberStrand® properties for 3 twisted fibers**

| Parameter | Value | Units |
|---|---|---|
| Modulus of elasticity ($E$) | 9.5 | N/m$^2$ |
| Cross sectional area ($A_{\text{braid}}$) | 0.9425 | mm$^2$ |
| Mass | 3.1 | g/m |

The modulus of elasticity is measured in the elastic region of tensile test results. The modulus of elasticity is related to a linear spring constant in the elastic region of the stress-strain curve with:

$$k_{\text{s}} = \frac{EA_{\text{braid}}}{L_o} \tag{4}$$

where $E$ is the modulus of elasticity, $A_{\text{braid}}$ is the cross sectional area of the braid of three twisted fibers, and $L_o$ is the un-stretched tether length.

### Solar Radiation Pressure

A simplified solar radiation pressure (SRP) model is used to quantify the capability of the TCS system to compensate for a constant external perturbation. The magnitude of the SRP force acting on a spacecraft is governed by the relationship[28]

$$F_{SRP} = P_{SR}C_R A_s \tag{5}$$

where $P_{SR}$ is the solar radiation pressure, $C_R$ is the surface reflectivity constant of the spacecraft, and $A_s$ is the surface area.

### Sample Force Magnitudes

To appreciate the expected force magnitudes a TCS structure will encounter on orbit, consider a two-node tethered system. With nodes of radius 0.5 m, separated by 2.5 m center to center and charged to a surface potential of 30 kV the expected force levels are shown in Table 2. The Coulomb force is computed with no plasma shielding, assuming a geostationary or deep space environment. The solar radiation pressure is computed at 1 Astronomical Unit (AU) from the sun where the solar radiation pressure is $4.56 \times 10^{-6}$ N/m, and the surface reflectivity is 1. It should be noted that at force equilibrium (without SRP) the nodes stretch apart only 1.1 mm.

## SINGLE-TETHER CONFIGURATION MODELING

This section documents the dynamic modeling of the single-tethered system. This model is reduced to two degrees of freedom that is linearized to obtain insight into potential motions about equilibrium.

*Syscom Advanced Materials, Inc. www.amberstrand.com, 1/15/2010

**Table 2. Expected force magnitudes for a two-node TCS separated by 2.5 m**

| Force | Value | Units |
|---|---|---|
| Coulomb ($F_c$) | 4.0 | mN |
| Tether ($F_s$) | 4.0 | mN |
| SRP ($F_{SRP}$) | 3.6 | $\mu$N |

### Two Degree of Freedom Model

A simplified two degree of freedom TCS model is developed to provide insight into how TCS node rotation impacts the charge requirements and related stiffness capabilities. While the numerical simulation can handle general translational and rotational motion of $N$ nodes, the results yield an overwhelming amount of data, making it difficult to gain any insight. The TCS model is based in deep space and features two nodes attached with a single-tether as shown in Figure 2.

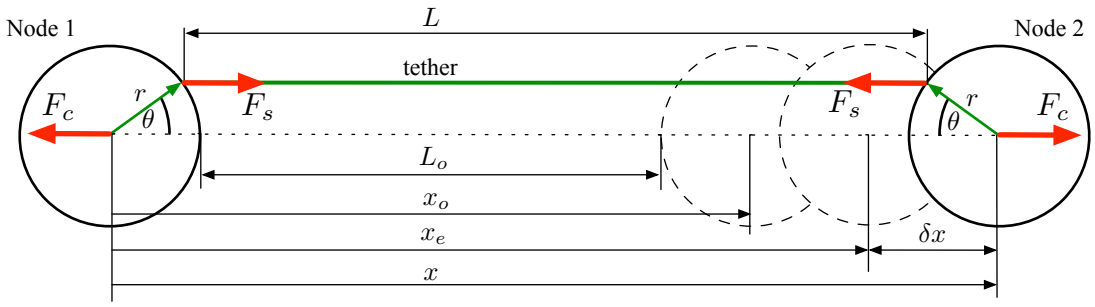


**Figure 2. Symmetric two-node system with two degrees of freedom**

By constraining the nodes to symmetrically rotate by an angle $\theta$ the tether remains parallel to the line of sight vector resulting in one dimensional translational motion with the Coulomb and Tether forces ($F_c$ & $F_s$) directly opposing each other. This reduces the model to one rotational degree of freedom and one translational. The Coulomb force for this model is assumed to have negligible shielding from the plasma environment due to the very small meter-level separation distances. This is a reasonable assumption given the force magnitude is reduced 0.02% at a separation of 10 meters in a 200 m Debye length plasma.

The translational equation of motion of this system is:

$$\ddot{x} = \frac{k_c Q}{m x^2} - \frac{k_s}{m}\left[x - x_o + 2r(1 - \cos\theta)\right] \tag{6}$$

where $L_o$ is the un-stretched tether length and $m$ is the node mass. With the tethers attached at fixed locations on the spherical surfaces any rotation will result in a torque on the node. This is modeled to examine the correlations between translational and rotational motions. The attitude is governed by the rotational equation of motion:

$$\ddot{\theta} = -\frac{r k_s}{I}\left[x - x_o + 2r(1 - \cos\theta)\right]\sin\theta \tag{7}$$

where $I$ is the mass moment of inertia of the modeled disk. For this two DOF model the mass of each node is equal and the mass moment of inertia of a solid disk is used. This is one property

that can be varied to analyze the effect of mass and its distribution on the dynamics of the system. For practical reasons, the simulation is restricted to attitude angles less than $\pm 90$ degrees to prevent tether entanglement.

**Single-Tether Linearized model**

Equation (6) has an equilibrium condition at a separation, $x = x_e$ and an attitude $\theta = 0$. The translational equation of motion is reduced to

$$\ddot{x} = 0 = \frac{k_c Q}{x_e^2} - k_s(x_e - x_o) \tag{8}$$

which can be arranged to a cubic relationship between the equilibrium distance $x_e$ and the associated charge product $Q$:

$$k_c Q = k_s(x_e - x_0)x_e^2 \tag{9}$$

Of the three $x_e$ solutions on the real solution is practical. At this equilibrium separation distance the Coulomb and tether forces are equal and the nodes remain stationary (with no external disturbances). One interesting consequence of this equilibrium distance is that it is independent of the system mass. The two DOF model given in Eqs. (6) and (7) is linearized about the equilibrium condition to produce a reduced system model to study the dynamic behavior of oscillations about the equilibrium states. Linearizing the translational motion for small departures ($\delta x = x - x_e$) results in:

$$\delta\ddot{x} \approx -\frac{1}{m}\left[\frac{2k_c Q}{x_e^3(Q)} + k_s\right]\delta x \tag{10}$$

This approximate translation description is decoupled from the angular rotation and is the form of the stable undamped harmonic oscillator equation. The natural frequency of this oscillatory translational response is given by:

$$\omega_T = \sqrt{\frac{1}{m}\left[\frac{2k_c Q}{x_e^3(Q)} + k_s\right]} \tag{11}$$

The rotational equation of motion is linearized to the form:

$$\ddot{\theta} \approx \frac{-rk_s}{I}\left[x_e(Q) - x_o\right]\theta \tag{12}$$

This linearized rotational equation of motion also decouples and is of the form of the stable undamped harmonic oscillator equation. The natural frequency of this oscillatory rotational response is given by:

$$\omega_R = \sqrt{\frac{rk_s}{I}\left[x_e(Q) - x_o\right]} \tag{13}$$

While these linearized models are only valid for small oscillations, in the results section they are shown to offer insight into the response of the system about its equilibrium state.

## SINGLE-TETHER SIMULATION RESULTS

The results of three studies providing insight into the dynamics and capabilities of the TCS concept are shown. Two case studies analyze the properties and motions of the linearized system model. The final case study demonstrates the TCS stiffening properties and capability to resist angular rate errors for various separation distances.

Each simulation case is run for at least one full oscillation in the attitude rotation, or stopped once the attitude goes beyond $\pm 90$ degrees. The TCS parameters common to each simulation case are shown in Table 3. The simulations are conducted with three single-tether configurations, each with a different un-stretched separation $x_o = 2.5, 5$, and 10 m, measured from center to center. The TCS motions are integrated using the full three-dimensional equations of motion detailed in the Appendix. The two-degree of freedom models developed here, provide verification of the full 3D model and simulation results.

**Table 3. Simulation Parameters Common For All Test Cases**

| Parameter | Value | Units |
|---|---|---|
| Initial attitude rate errors ($\dot{\theta}_0$) | 1-90 | deg/min |
| Voltage range ($V$) | 5-50 | kV |
| Spacecraft separations ($x_o$) | 2.5, 5, 10 | m |
| Spacecraft node mass ($m$) | 50 | kg |
| Spacecraft node radius ($r$) | 0.5 | m |

### Natural Frequency Response of the Linearized Model

Using the linearized models of Equations 10 and 12 and the system properties of Table 3, it is possible to gauge the expected stiffness of the TCS. The natural frequency of the linearized translational and rotational motions of Equations 11 and 13 is a measure of the TCS stiffness. Figure 3 shows the natural frequency of the linearized translational motion for three separation distances. For the voltage range analyzed, the natural frequency of the response is essentially independent of the spacecraft charge. The values change by less than 0.1%, indicating the translational stiffness is largely determined by the tether material stiffness. As the separation distance between the nodes decreases, the frequency of the system response increases due to the increased stiffness of shorter tethers.

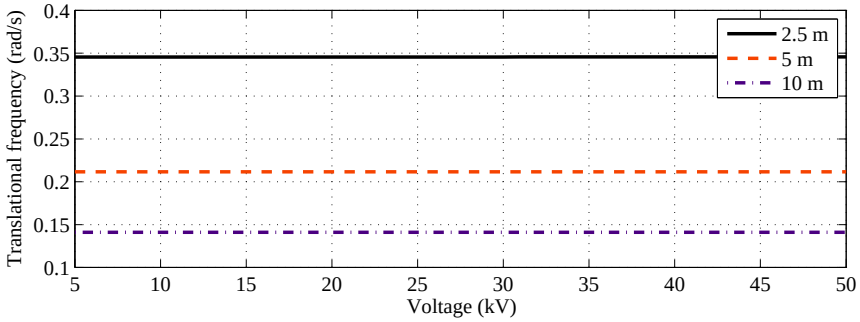


**Figure 3. Natural frequency of linearized translational motion**

Figure 4 shows the natural frequency of the linearized rotational motion, from Equation 13, for three separation distances. In contrast to the translational stiffness which is essentially decoupled from the magnitude of the electrostatic inflation force (assuming AmberStrand®-like materials), the rotational stiffness or natural frequency is directly related to the TCS nodal potentials.

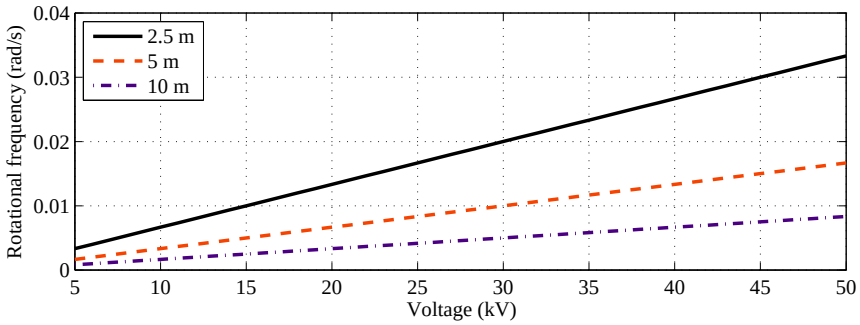


**Figure 4. Natural frequency of linearized rotational motion**

Note that the translational natural frequency is approximately an order of magnitude greater than the corresponding rotational motion. For these uncoupled linearized systems and the system parameters analyzed this implies that the system will better constrain translational motion.

### Impact of Tether Material on Rotational Motion

The linearized models are used to analyze the effect of varying the tether material stiffness (spring constant) $k_s$ on the resulting rotational node motion. Equation 12 has the solution $\theta(t) = A\sin(\omega_R t + \phi)$ where the amplitude of oscillation $A$ is defined as:

$$A = \frac{2mr\dot{\theta}_0}{5}\underbrace{\left[\frac{1}{k_s\left(x_e(Q,k_s) - x_o\right)}\right]}_{\alpha} = \frac{2mr\dot{\theta}_0}{5}\alpha \tag{14}$$

Here $\dot{\theta}_0$ is the initial angular rate and $\theta_0$ is assumed to be zero. The amplitude $A$ is proportional to $\alpha$, which depends on the tether stiffness $k_s$ and node charge product $Q$. Note that $x_e$ is a function of $k_s$ so amplitude is not inversely proportional to the spring constant. For a 10 m separated system using the nominal AmberStrand® braid the spring constant is $k_s = 0.995$. In this study this spring constant is varied in value from $k_s \times 10^{-5}$ through $k_s \times 10$, simply to investigate the impact of a range of material properties on the rotational stiffness. The resulting amplitude multiplication factor, $\alpha$, of equation14 is shown in Figure 5.

This study indicates that changes in the tether spring constant have a minimal effect on the overall amplitude of angular rotations. It requires a spring constant that is reduced by 100,000 times the value of the 10 m separated case and nodes of 50 kV to increase the maximum angular rotation by five.

### Impact of Tether Length Variations on the Rotational Stiffness

After deployment the TCS nodes will not be perfectly at rest with respect to each other. This analysis uses the full 3D non-linear equations of motion (see Appendix) to demonstrate the ability of the Coulomb force to stiffen the structure and resist deformation due to a small initial angular

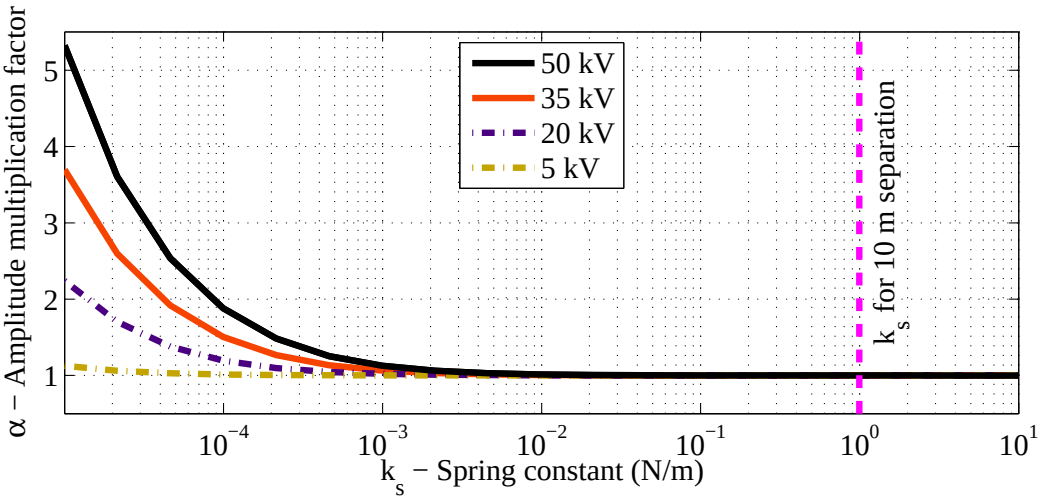


**Figure 5. Effect of varying tether spring constant on the amplitude of linearized angular oscillations**

rate. Three two-node, single-tether configurations of different separations distances are simulated with symmetric initial angular rotations. Here both nodes perform the same (but opposite) rotation and consequently equivalent translational motion.

Figure 6 shows the maximum attitude angle that is reached by the nodes for each separation distance case and initial angular rate error. This is shown as a function of the spacecraft surface voltage. No material damping is considered in this study as the focus is on issues with tethers wrapping up on nodes after a single oscillation. The weak material damping would only impact long-term oscillation amplitudes.

Also shown in Figure 6 is what conditions will cause the tether to go slack. The solid lines indicate that the tether remains taut for the simulation duration, where as the dashed regions have the tether reach a slack state. For many of these conditions the tether may go slack only a small fraction of the simulation time and is typically less than a millimeter from the un-stretched tether length. This is a concern as the nodes are no longer at their desired separation distance and the tether may undergo detrimental impact loads if the dynamics cause a sudden repulsion. For the three separation cases analyzed the conditions that cause the angle of rotation to go above 27° will result in a slack tether. Note that this rotation amplitude limit is dependant on the initial conditions considered.

A reduction in the spacecraft separation distance results in two key changes on the system as shown in Figure 6. Firstly, the tether spring constant increases and secondly the spacecraft will be closer together, increasing the Coulomb force for an equivalent charge level. This increases the stiffening of the rotational motion, as indicated by the earlier linear analysis. This simulation now quantifies the enhanced ability of a stiffened TCS to resist deformation due to an initial angular rate error on the nodes. Figure 6(a) shows that a 10 meter nodal separation with 35 kV potentials requires an initial nodal rotation rate less than 10 deg/min, a small value. Otherwise, the tethers will go slack at times, or the nodes could wrap up with the tethers. In contrast, Figure  shows that reducing the separation to 2.5 m and maintaining a 35 kV potential will constrain a 40 deg/min angular rate. Shorter separation distances yield significant increases to the rotational stiffness of the TCS nodes.

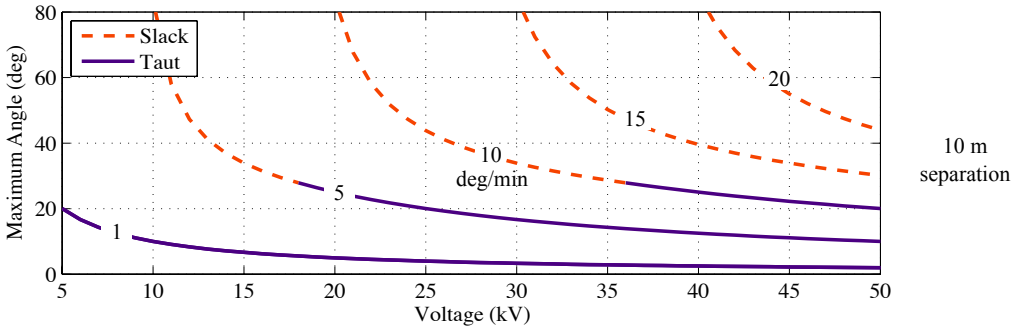


(a) Maximum angle for 10 m separated nodes

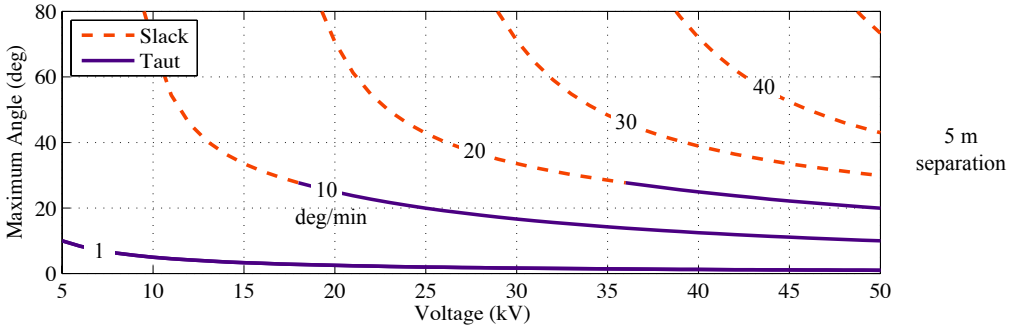


(b) Maximum angle for 5 m separated nodes

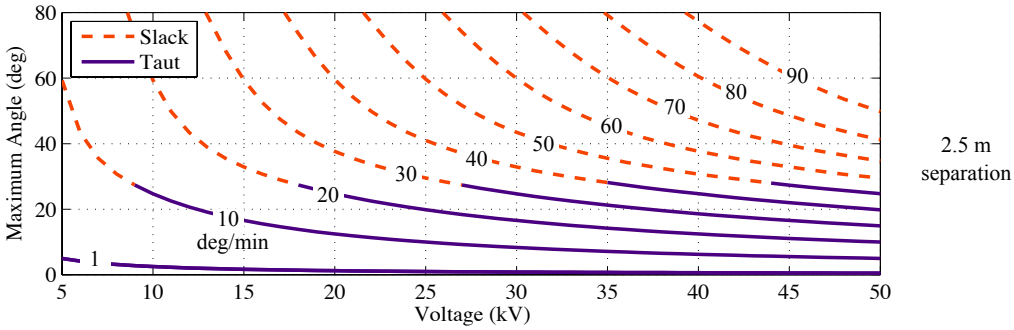


(c) Maximum angle for 2.5 m separated nodes

**Figure 6. Maximum attitude reached as a function of initial attitude rate error**

An alternate method of showing the maximum angle reached for this two-node configuration is with the contour plots of Figure 7. Once again, the rotations are limited to $\pm 90$ degrees, the limit of node wrap up. Note that slack line conditions are not illustrated here, but are simulated. These plots again illustrate how the rotational stiffness can be increased with shorter tether lengths. Large separation distances of 10 meters are shown to be challenging with dozens of kilo-Volt potentials, as shown with the large area of 90 deg attitudes in Figure 7(a). Instead, the TCS is practical with shorter meter level separations as illustrated with the larger operational area of Figure .

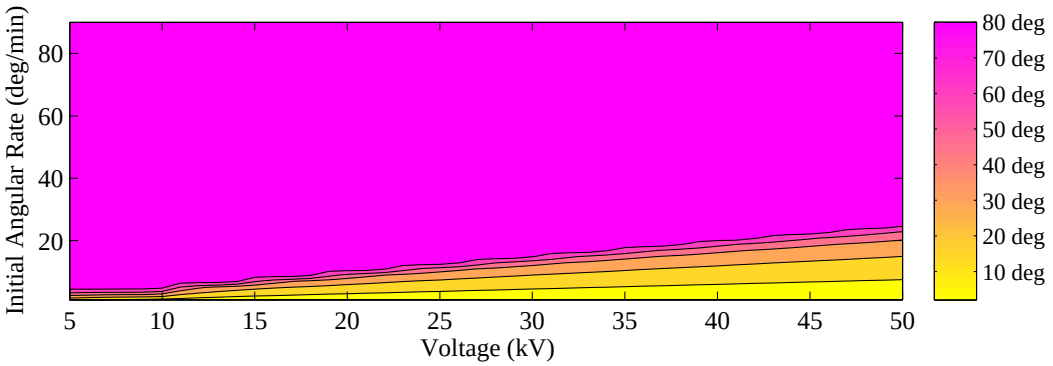


(a) Contour plot of maximum angle for 10 m separated nodes

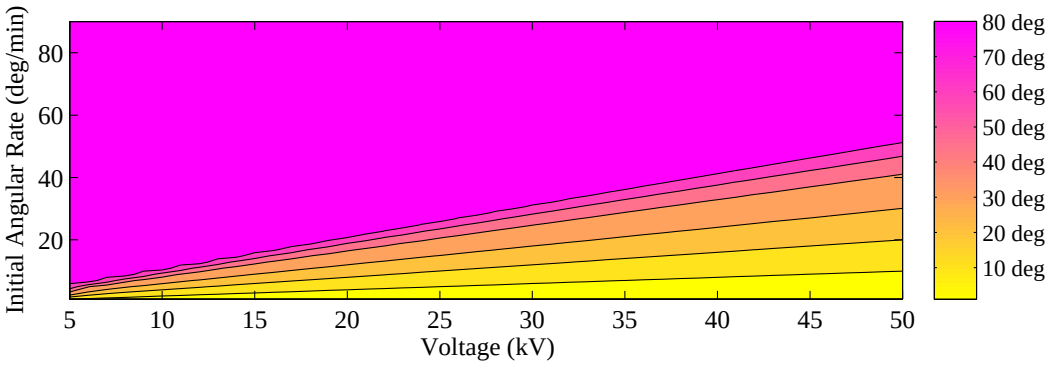


(b) Contour plot of maximum angle for 5 m separated nodes

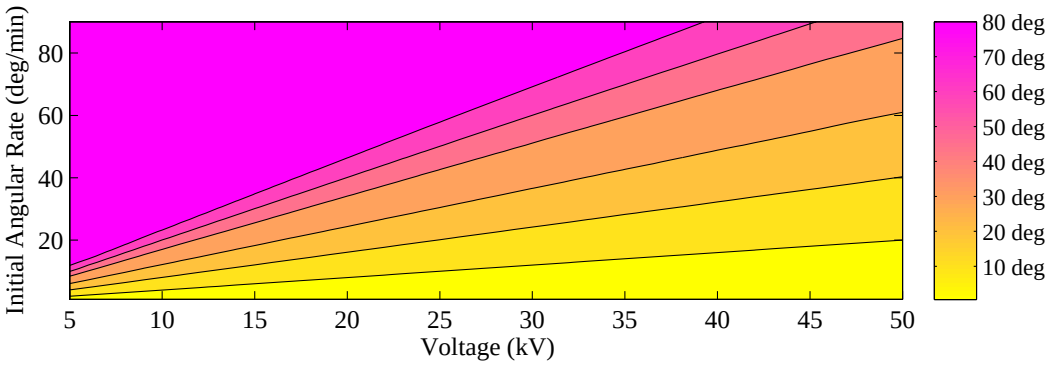


(c) Contour plot of maximum angle for 2.5 m separated nodes

**Figure 7. Contour plot of maximum attitude reached as a function of initial attitude rate error**

## SOLAR RADIATION PRESSURE DISTURBANCE RESPONSE

At GEO, where the TCS concept is to be operated, solar radiation pressure (SRP) can play a significant role as a disturbance force on the inertial orbital motion of satellites.[29] The intent of the following study is to quantify the capabilities of the two-node TCS configuration to resist deformation from an external perturbation.

### Solar Radiation Pressure Model

The same single-tether configuration operating in deep space is used as a baseline model. The solar radiation pressure is added as a bias force that is compressing the system along the direction of the tether line as shown in Figure 8. The SRP force is acting on both nodes, but increasing the size of node 1 produces a differential SRP that attempts to compress the nodes. The concern is wether the Coulomb forces are large enough to maintain tension in this setup. The parameters of the study are shown in Table 4.

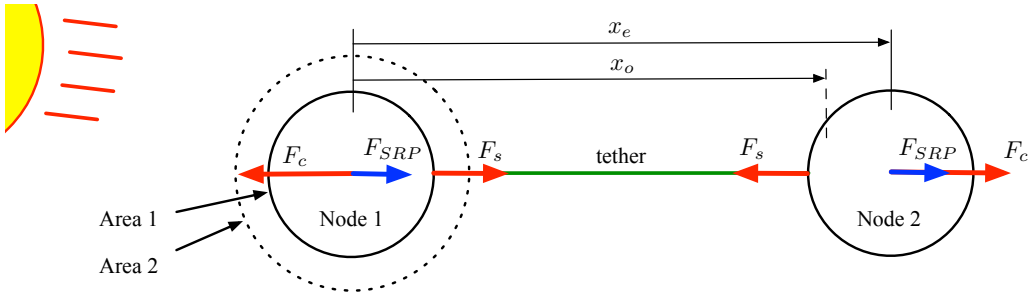


**Figure 8. Two-node, 2DOF Solar radiation pressure model**

**Table 4. Case 3 Simulation Parameters**

| Parameter | Value | Units |
|---|---|---|
| Spacecraft Area Ratios ($A_s$) | 1-10 | |
| Spacecraft node radius ($r$) | 0.5 | m |
| Spacecraft separation ($x_o$) | 10 | m |
| Solar pressure (1 AU) | $4.56\times10^{-6}$ | N/m |
| Surface reflectivity | 1 | |

Only one node separation of 10 m is used, as this is the worst case scenario of the three separation distance configurations analyzed earlier. If the Coulomb forces are found to be sufficient to maintain tension for this challenging larger separation distance, then TCS systems of shorter separation distances should not be significantly compressed by differential SRP. The sunlit surface area of node 1 is increased linearly in multiples from one to ten, where one is the nominal surface area corresponding to a 0.5 meter radius circle. An increase in the surface area will cause the homogeneously distributed charge to also increase for a fixed nodal potential. This would further increase the stiffening capabilities of the TCS system. To maintain a worst-case scenario, this model does not incorporate any change in the Coulomb force as the surface area of node 1 is increased.

### TCS Compression Due to Differential Solar Radiation Pressure

The numerical simulation is set up with the craft initially at their undisturbed equilibrium states. The contour plot of Figure 9 shows what the worst-case percentage of the buffer between equilibrium distance and un-stretched distance is compromised by the SRP disturbed relative motion. This value is calculated using:

$$\% = \frac{L_e - \min(L)}{L_e - L_o} 100 \tag{15}$$

This indicates how close the tether length is from becoming slack as a function of both charge and the surface area ratio between the craft. The top left portion of the figure indicates that the crafts relative motion compress to the point of causing the tether to go slack at times.

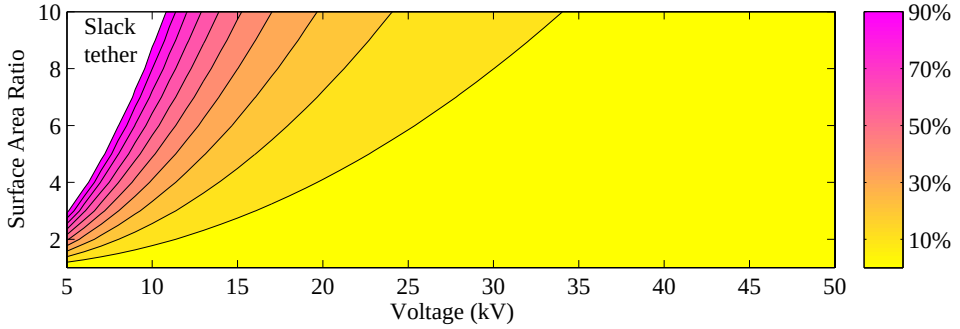


**Figure 9. Tether distance from becoming slack under varying SRP disturbances**

As indicated in Figure 9 an increase in charge will stiffen the system to resist perturbations. For shorter separation distances of less than 10 meters the system is further stiffened reducing the voltage requirements to resist the same disturbance force levels. Note that even with a very large TCS node size ratio of 10 and 25 kV potential, the compression due to this worst-case alignment of the differential SRP disturbance would only cause approximately a 20% compression of the equilibrium distance buffer. For TCS separation distances on the meter level, considering near equal nodal sizes, the differential SRP will have a minimal impact on the TCS shape.

## DOUBLE TETHER CONFIGURATION

Having a TCS system that incorporates a redundant set of tethers between the nodes, with the attachment points distributed across the nodes surface, is a method of increasing the rotational TCS node stiffness. The following numerical simulation results quantify by how much the rotational TCS node stiffness can be increased if a double-tether setup is employed.

### Two Degree of Freedom Model

A development for the TCS concept is a double-tethered craft system as shown in Figure 10. The intent of the redundant double-tether is to induce additional rigidity and resistance to deformation to the TCS. The system is modeled with symmetric motions so that it can once again be reduced to two degrees of freedom to gain analytical insight.

The translational equations of motion of the symmetric double-tether system is:

$$\ddot{x} = \frac{k_c Q}{m x^2} - \frac{2k_s}{m}\left[x - x_o + 2r\cos\phi(1-\cos\theta)\right] \tag{16}$$

where $\phi$ is the half angle between the tether attachment points. The rotational equation of motion is given by:

$$\ddot{\theta} = -\frac{2rk_s\sin\theta}{I}\left\{\cos\phi(x-x_o) + 2r\left[\cos\theta + \cos^2\phi - 2\cos\theta\cos\phi\right]\right\} \tag{17}$$

The rotational equation of motion is significantly more complex than the single-tether setup. However, linearizing the double-tether motions about the equilibrium states, still produces a decoupled

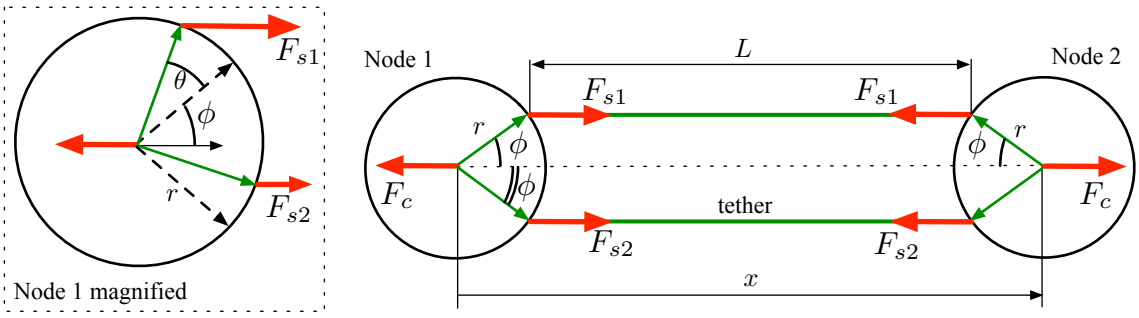


**Figure 10. Two node system with double-tether**

set of equations. The translational motion for small departures about the equilbrium ($\delta x = x - x_e$) is:

$$\delta\ddot{x} \approx -\frac{2}{m}\left[\frac{k_c Q}{x_e^3(Q)} + k_s\right]\delta x \tag{18}$$

This linearized translational motion is of the form of a stable undamped harmonic oscillator. It is also equivalent to the single-tether case of Equation 10 with the additional factor of two. This increases the natural frequency and stiffness of the translational response. The rotational equation of motion is linearized to the form:

$$\ddot{\theta} \approx \frac{-2rk_s}{I}\left[(x_e(Q) - x_o)\cos\phi + 2r(1-\cos^2\phi)\right]\theta \tag{19}$$

This linearized rotational equation of motion decouples from the translational motion and is a stable undamped harmonic oscillator equation. Unlike the single-tether rotational motion of Equation 12 this linearization features a factor of two as well as dependance on the tether attachment angle $\phi$. Figure 11 plots the natural frequency of Equation 19 as a function of charge and tether attachment angle. This figure shows how stiffening is increased with the tether angle $\phi$. This geometric stiffening is a consequence of the larger moment arm acting on the node from equilibrium. The data in this figure is generated with nodes of 0.5 m radius and separated by 2.5 m.

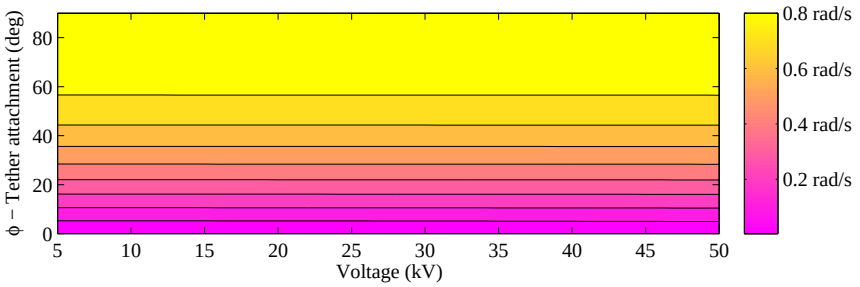


**Figure 11. Natural frequency of linearized rotational motion of double-tether model**

Figure 4 showed for the single-tether case that increasing charge increases the natural frequency of the rotational response. This also occurs with the natural frequency of the double-tether shown in Figure 11, however has less contribution than the geometric stiffening. Utilizing a double-tether will increase the ability to resist nodal angular rotations.

### Double Tether System Response to Angular Rate Errors

In this simulation case the double-tether response to angular rate errors is compared to that of a single-tether configuration. A two-node configuration with a separation of 2.5 m is analyzed. The simulation is performed using the full 3D and non-linear coupled equations of motion. The parameters of the symmetric simulation are shown in table 5.

**Table 5. Double Tether Simulation Parameters**

| Parameter | Value | Units |
|---|---|---|
| Initial attitude rate errors ($\dot{\theta}_0$) | 1-2 | deg/min |
| Spacecraft node radius ($r$) | 0.5 | m |
| Spacecraft separation ($x_o$) | 2.5 | m |
| Tether attachment point angle ($\phi$) | 20 | deg |

Using two initial angular rate errors for each tethered system the resulting maximum attitude angle reached is shown in Figure 12 on a y-axis log plot. There is a noticeable difference in the systems responses. The double-tethered system performing better at reducing maximum rotation due to initial rate errors. The results indicate that the resulting moment arm from the double-tether configuration significantly increases the systems response to angular rates. While the double-tether system has the advantage of producing a stiffer system, it is also prone to having a tether go slack as shown by the dashed lines in the figure. This can be overcome by maintaining a higher, yet realistic, charge level. In contrast, during this simulation case the single-tether system remains taut for any charge level, at a cost of reaching attitude angles at least a magnitude higher.

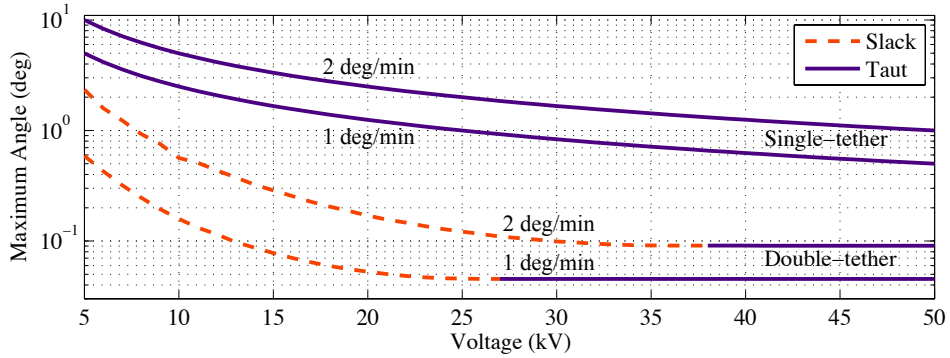


**Figure 12. Double-tether vs single-tether attitude response to angular rate errors**

The results of this simple double-tether simulation indicate that a TCS system can be significantly stiffened beyond an equivalent single-tether system. This offers enhanced capabilities to resist disturbance or deployment motions. An additional advantage is the safety provided by having two tethers on the system. In case one tether is severed, the remaining tether would still maintain the TCS shape, although with reduced accuracy. Future work will investigate three dimensional TCS configurations to consider more complex multi-tether nodal connections.

## CONCLUSIONS

The novel TCS concept offers unique on-orbit advantages. Large space structures are envisioned that can be launched in a low-mass and compact configuration and deployed and resized once on orbit. To advance the concept, this study analyzes the complex relative motion of the closely operated tethered spacecraft nodes. Results are produced by implementing the full three dimensional non-linear equations of motion that incorporate the coupling forces of the attitudes of each spacecraft in the TCS formation. Future studies will incorporate alternate tether materials and models.

The results of this dynamical motion study indicate that a TCS will inflate under Coulomb forces and with increased charge will become quasi-rigid and resist deformation from external forces. It is shown that for realistic and achievable charge levels a TCS can maintain both its shape and its tethers in tension under the influence of disturbances such as initial nodal angular rate errors and compressive solar radiation pressure at GEO. This algorithms versatility and ability to examine any general TCS system will lead to numerous future investigations exploring the operating feasibility of the TCS concept.

## ACKNOWLEDGEMENT

The authors would like to thank the Aerospace Engineering Sciences senior design team, *CTS - CubeSat Tether System*, for the AmberStrand® material properties.

## APPENDIX - THREE DIMENSIONAL TCS MODELING

The simplified two degree of freedom TCS models offer insight into translational and rotational motion. Shown here is the development of the full three dimensional non-linear equations of motion that can accommodate general TCS spacecraft configurations. The algorithm simulates the TCS in deep space, or under the gravitational attraction of orbit and incorporates external disturbance forces. Although not performed in this study, the intent of this simulator is to fully explore the capabilities and operating regimes of the TCS along with a study of its dynamic behavior under realistic disturbance environments.

The algorithm is general to accommodate TCS relative motion studies featuring any number of nodes and tethers in any initial orbit configuration. The location of each spacecraft node, $\boldsymbol{R}_i$, is defined in a Earth centered inertial (ECI) frame as defined in Figure 13.

At epoch each nodes body frame is aligned with the ECI frame. The relative separation of each nodes center $\rho_{ij}$ at epoch defines the desired separation distances. The relative alignment of each node at epoch also defines the tether connection point at each nodes spherical surface. The tether connection point lies on the straight line between each nodes center point. It is not necessary to have a tether connecting each node as a tether connection matrix, $[K_{ij}]$, defines which nodes are connected.

### Tether Force

The separation of the nodes spherical surface at epoch defines the desired tether length $x_{ij} = \rho_{ij}(0) - 2r$. The tethers are modeled as linear springs that are stretched beyond this optimal length from either the nodal relative motion or from attitude rotations as shown in Figure 14. The tether length increase is defined by $\delta x_{ij}$ and the resulting tensile force acting on node $i$ from the tether

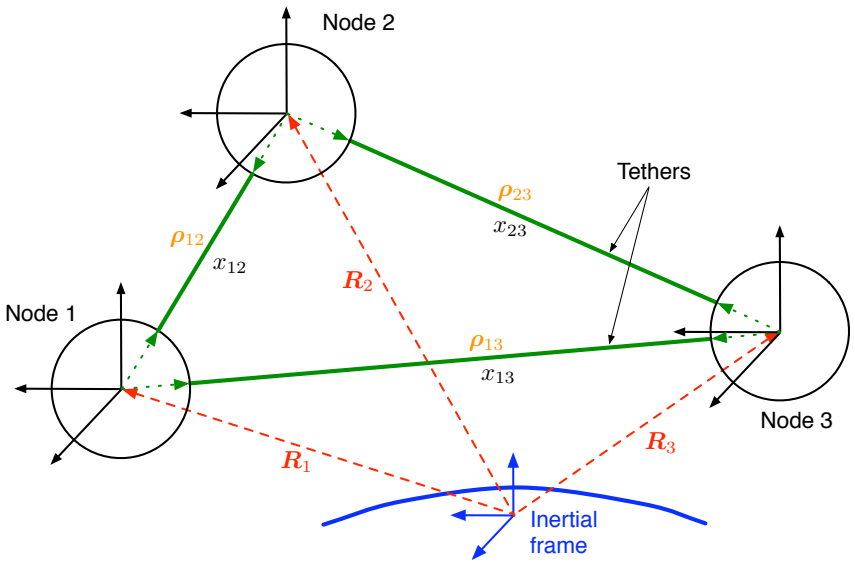


**Figure 13. Dynamic model setup for a three craft example**

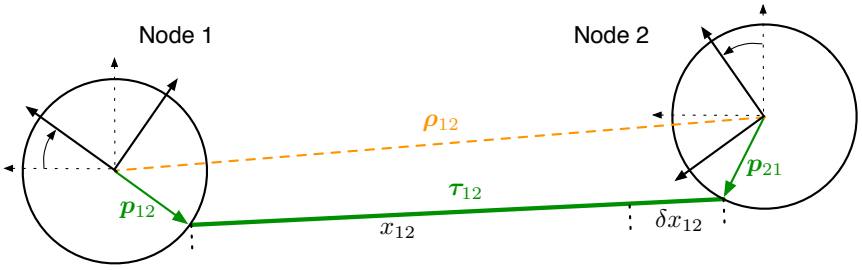


**Figure 14. Two node example of attitude change and increased tether length**

connected to node $j$ is:

$$\boldsymbol{T}_{ij} = k_{\mathrm{s}} \delta x_{ij} \hat{\boldsymbol{\tau}}_{ij} \tag{20}$$

where $\boldsymbol{\tau}_{ij}$ is the vector defining the tether connecting node $i$ to $j$. When the tether length is shorter than desired, the tether goes slack and there is no force acting on the corresponding nodes.

### Translational Equation of Motion

Using the Coulomb force of equation 1, tensile force and the gravitational force, the resulting equations of motion of each node is calculated using:

$$\ddot{\boldsymbol{R}}_i = -\frac{\mu}{|\boldsymbol{R}_i|^2}\hat{R}_i + \sum_{j=1}^{N} K_{ij}\frac{\boldsymbol{T}_{ij}}{m_i} + \sum_{j=1}^{N} \frac{k_c q_i q_j (-\hat{\boldsymbol{\rho}}_{ij})}{m_i \rho_{ij}^2} e^{-\rho_{ij}/\lambda_d}\left(1 + \frac{\rho_{ij}}{\lambda_d}\right) \quad , \quad i \neq j \tag{21}$$

where $\mu = 3.986 \times 10^{14}$ m$^3$s$^{-2}$ is the gravitational coefficient for Earth, $m_i$ is the spacecraft node mass, $N$ is the total number of nodes in the TCS model. Note that these charges do not influence the relative motion. They simply provide an inflating force, relative to the systems center of mass, that

increases the tether tensions. The scalars $K_{ij}$ are the tether connection matrix components which define which nodes are connected by a tether. The motion of each node is propagated in time using a variable step Runge-Kutta algorithm. A external disturbance force is added as an inertial vector to Equation 21.

### Nodal Rotational Equation of Motion

The attitude of each spacecraft node is also propagated by computing the torque acting on the node from each tether:

$$^{\mathcal{B}}\mathbf{\Gamma}_i = \sum_{j=1}^{N} \left( K_{ij} {}^{\mathcal{B}}\boldsymbol{p}_{ij} \times [\mathcal{BI}]_i {}^{\mathcal{I}}\boldsymbol{T}_{ij} \right) \quad , \quad i \neq j \tag{22}$$

Where $\boldsymbol{p}_{ij}$ is the body fixed vector that defines the location of the tether connection point on node $i$ that connects to node $j$ and $[\mathcal{BI}]_i$ is the direction cosine matrix of the attitude of node $i$ relative to the inertial frame. The angular acceleration of each node is defined in the body frame with Euler's rotational equations of motion:[30]

$$[I]\dot{\boldsymbol{\omega}}_i = -\boldsymbol{\omega}_i \times ([I]\boldsymbol{\omega}_i) + \mathbf{\Gamma}_i \tag{23}$$

The attitude of each node is represented with the modified Rodrigues parameters (MRP) which are integrated using the differential kinematic equation:

$$\dot{\boldsymbol{\sigma}}_i = \frac{1}{4}\left[(1-\sigma_i^2)[I_{3x3}] + 2[\tilde{\boldsymbol{\sigma}}]_i + 2\boldsymbol{\sigma}_i\boldsymbol{\sigma}_i^T\right]\boldsymbol{\omega}_i \tag{24}$$

The MRP set will go singular with a rotation of $\pm 360^\circ$. To ensure a non-singular description, the MRP description is switched to the shadow set whenever $|\boldsymbol{\sigma}| > 1$.[30]

## REFERENCES


[1] R. E. Freeland, G. D. Bilyeu, , G. R. Veal, and M. M. Mikulas, "Inflatable Deployable Space Structures Technology Summary," *49th International Astronautical Congress*, Melbourne, Australia, Sept. 28 – Oct. 2 1998.

[2] R. G. Cobb, S. N. Lindemuth, J. C. Slater, and M. R. Maddux, "Development and Test of a Rigidizable Inflatable Structure Experiment," *45th AIAA/ASME/ASCE/AHS/ASC Structures, Structural Dynamics & Materials Conference*, Palm Springs, CA, April 19–22 2004. Paper No. AIAA 2004–1666.

[3] P. A. Tarazaga, D. J. Inman, and W. K. Wilkie, "Control of a Space Rigidizable Inflatable Boom Using Macro-fiber Composite Actuators," *Journal of Vibration and Control*, Vol. 13, No. 7, 2007, pp. 935–950.

[4] H. Fang, K. Knarr, U. Quijano, J. Huang, and M. Thomson, "In-space Deployable Reflectarray Antenna: Current and Future," *AIAA/ASME/ASCE/AHS/ASC Structures, Structural Dynamics and Materials Conference*, Schaumburg, IL, April 7-10 2008.

[5] K. G. Carpenter, C. J. Schrijver, M. Karovska, and S. M. C. D. Team, "The Stellar Imager (SI) Project: A Deep Space UV/Optical Interferometer (UVOI) to Observe the Universe at 0.1 Milli-arcsec Angular Resolution," *Proceedings of the NUVA Conference*, El Escorial, Spain, June 2007.

[6] G. Blackwood, C. Henry, E. Serabyn, S. Dubovitsky, M. Aung, and S. M. Gunter, "Technology and Design of an Infrared Interferometer for the Terrestrial Planet Finder," *AIAA Space 2003*, Long Beach, CA, Sept. 23–25 2003. Paper No. AIAA 2003-6329.

[7] J. R. Wertz, "High Resolution Structureless Telescope," Tech. Rep. MC04-1643, NASA/NIAC, April 26 2004.

[8] R. Hyde, S. Dixit, A. Weisberg, and M. Rushford, "Eyeglass: A Very Large Aperture Diffractive Space Telescope," *Highly Innovative Space Telescope Concepts*, 2002.

[9] R. Hyde, "Eyeglass Large Aperture, Lightweight Space Optics," Tech. Rep. UCRL-ID-151390, University of California, Lawrence Livermore National Laboratory, Feb. 10 2003.

[10] L. B. King, G. G. Parker, S. Deshmukh, and J.-H. Chong, "Spacecraft Formation-Flying using Inter-Vehicle Coulomb Forces," tech. rep., NASA/NIAC, January 2002.

[11] D. W. Miller, , R. J. Sedwick, E. M. C. Kong, and S. Schweighart, "Electromagnetic Formation Flight for Sparse Aperture Telescopes," *IEEE Aerospace Conference Proceedings – Volume 2*, Big Sky, Montana, March 9–16 2002.

[12] J. Gersh, "Architecting the Very-Large-Aperture Flux-Pinned Space Telescope: A Scalable, Modular Obtical Array with High Agility and Passively Stable Orbital Dynamics," *AAS/AIAA Astrodynamics Specialist Conference*, Honolulu, Hawaii, Aug. 18–21 2008.

[13] C. R. Seubert and H. Schaub, "Tethered Coulomb Structures: Prospects and Challenges," *AAS F. Landis Markley Astrodynamics Symposium*, Cambridge, MA, June 30 – July 2 2008. Paper AAS 08–269.

[14] L. B. King, G. G. Parker, S. Deshmukh, and J.-H. Chong, "Study of Interspacecraft Coulomb Forces and Implications for Formation Flying," *AIAA Journal of Propulsion and Power*, Vol. 19, May–June 2003, pp. 497–505.

[15] A. Natarajan and H. Schaub, "Linear Dynamics and Stability Analysis of a Coulomb Tether Formation," *AIAA Journal of Guidance, Control, and Dynamics*, Vol. 29, July–Aug. 2006, pp. 831–839.

[16] A. Natarajan, H. Schaub, and G. G. Parker, "Reconfiguration of a Nadir-Pointing 2-Craft Coulomb Tether," *Journal of British Interplanetary Society*, Vol. 60, June 2007, pp. 209–218.

[17] S. G. Tragesser and A. Tuncay, "Orbital Design of Earth-Oriented Tethered Satellite Formations," *Journal of the Astronautical Sciences*, Vol. 53, Jan. – March 2005, pp. 51–64.

[18] C. Menon and C. Bombardelli, "Self-Stabilising Attitude Control for Spinning Tethered Formations," *Acta Astronautica*, Vol. 60, 2007, pp. 828–833.

[19] V. V. Beletsky and E. M. Levin, *Dynamics of Space Tether Systems*, Vol. 83. American Astronautical Society, 1993. Advances in the Astronautical Sciences.

[20] M. L. Cosmo and E. C. Lorenzini, "Tethers in Space Handbook," tech. rep., NASA Marshall Space Flight Center, December 1997.

[21] J. Berryman and H. Schaub, "Static Equilibrium Configurations in GEO Coulomb Spacecraft Formations," *AAS/AIAA Spaceflight Mechanics Meeting*, Copper Mountain, CO, Jan. 23–27 2005. Paper No. AAS 05–104.

[22] H. Vasavada and H. Schaub, "Analytic Solutions for Equal Mass Four-Craft Static Coulomb Formation," *Journal of the Astronautical Sciences*, Vol. 56, Jan. – March 2008, pp. 7–40.

[23] A. Natarajan and H. Schaub, "Hybrid Control of Orbit Normal and Along-Track 2-Craft Coulomb Tethers," *AAS/AIAA Spaceflight Mechanics Meeting*, Sedona, AZ, Jan. 28–Feb. 1 2007. Paper AAS 07–193.

[24] S. Wang and H. Schaub, "One-Dimensional 3-Craft Coulomb Structure Control," *7th International Conference on Dynamics and Control of Systems and Structures in Space*, Greenwich, London, England, July 16–20 2006, pp. 269–278.

[25] S. Wang and H. Schaub, "Switched Lyapunov Function Based Coulomb Control of a Triangular 3-Vehicle Cluster," *AAS/AIAA Astrodynamics Specialist Conference*, Pittsburgh, PA, Aug. 9–13 2009.

[26] T. I. Gombosi, *Physics of the Space Environment*. New York, NY: Cambridge University Press, 1998.

[27] H. Schaub, G. G. Parker, and L. B. King, "Challenges and Prospect of Coulomb Formations," *Journal of the Astronautical Sciences*, Vol. 52, Jan.–June 2004, pp. 169–193.

[28] D. A. Vallado, *Fundamentals of Astrodynamics and Applications*. Space Technology Library, Springer, 3rd ed., 2007.

[29] S. Valk, A. Lemaitre, and F. Deleflie, "Semi-analytical theory of mean orbital motion for geosynchronous space debris under gravitational influence," *Advances in Space Research*, Vol. 43, No. 7, 2009, pp. 1070–1082.

[30] H. Schaub and J. L. Junkins, *Analytical Mechanics of Space Systems*. Reston, VA: AIAA Education Series, October 2003.